Supporting information for

Ultrafine nickel nanoparticles encapsulated in N-doped carbon promoting hydrogen oxidation reaction in alkaline media

Jie Wang†[1], Xue Dong†[2], Jing Liu*[1], Wenzhen Li[3], Luke T Roling[3], Jianping Xiao*[2], Luhua Jiang*[1]

[1] Electrocatalysis & Nanomaterial Laboratory, College of Materials Science & Engineering, Qingdao University of Science & Technology, Qingdao, 266042, P.R. China

[2] Dalian Institute of Chemical Physics, Chinese Academy of Sciences, Dalian, 116023, P.R. China.

[3] Department of Chemical & Biological Engineering, Iowa State University, Ames, IA 50011-1098, Unites States.

† These authors contributed equally to this work.

*Corresponding authors: liuj955@qust.edu.cn (J. L.); xiao@dicp.ac.cn (J. X.); luhuajiang@qust.edu.cn (L. J.)

Experimental Section

Chemicals and Materials

Nickel Chloride hexahydrate ($NiCl_2 \cdot 6H_2O$, Sinopharm Chemical Reagent Co. Ltd. ≥ 98%), sodium hydroxide (NaOH, Sinopharm Chemical Reagent Co. Ltd. ≥ 96%) Ethylene Glycol ($C_2H_6O_2$, Sinopharm Chemical Reagent Co. Ltd. ≥ 99.8%), trisodium citrate dihydrate ($C_6H_5Na_3O_7 \cdot 2H_2O$, Sinopharm Chemical Reagent Co. Ltd. ≥ 98%), polyethylene imine (Sigma-Aldrich Co., Mw 25000), hydrochloric acid (HCl, Yantai Far Eastern Fine chemical Co. Ltd.), ethanol absolute (CH_3CH_2OH, Sinopharm Chemical Reagent Co. Ltd. ≥ 99.8%), potassium hydroxide(KOH, Sinopharm Chemical Reagent Co. Ltd. ≥85%) and Nafion 117 solution (Sigma-Aldrich Co., 5.w.t.%) were used as received without any further purification.

Preparation of polyethylene imine modified XC (PEI-XC)

Vulcan XC was firstly subjected to acidic treatment by refluxing in 5M HNO_3 at 120°C for 6h. The precipitate was collected and washed to pH=7 by copious of deionized water. After dried in an oven at 120°C for 8h, the carbon black was obtained to use as the support and denoted as XC. For PEI modification, typically, 500 mg of XC were dispersed homogenously in a 1 w.t.% PEI aqueous solution. The mixture was then stirred magnetically at ambient for 8h. After that, the black powder was filtrated, washed by deionized water and then dried. The obtained carbon black was denoted as PEI-XC.

Synthesis of Ni/XC

Ni/XC catalyst was synthesized referred to a polyol reduction method.[1] Briefly, 0.174g of $NiCl_2 \cdot 6H_2O$ and 0.36g of $C_6H_5Na_3O_7 \cdot 2H_2O$ were dissolved in 30 mL of ethylene glycol (EG). Then 6 mL of 5w.t.% NaOH EG solution was added. The above solution was heated to 170°C to react for 20h. After cooling down to room temperature, 50mg of XC were added, followed by adding 0.8mL 1M HCl ethanol solution. The mixture was kept stirring for 6h. After that, the precipitate was collected by centrifugation and washed with ethanol. After dried in a vacuum oven, the sample was subjected to a thermal-treatment in a tube furnace heating to 370°C in nitrogen atmosphere for 1h. The obtained product was denoted as Ni/XC.

Synthesis of Ni/PEI-XC

Ni/PEI-XC was synthesized by the same procedure as that for Ni/XC, except the PEI-XC was adopted as the support.

Synthesis of Ni@NC/PEI-XC

110 mg of the as prepared pre-thermal treated Ni/PEI-XC were dispersed in 50 mL of 10 mmol tris-HCl buffer (pH = 8.5) solution. Then, 100 mg of dopamine were added and stirred for different time periods of 5min, 15min, 30min, and 60min, respectively. After that, the precipitate was obtained after filtrated and washed by deionized water. After drying, the powder was transferred to a tube furnace and heated to 400^{o}C for 2h in the N_2 atmosphere. The product was denoted as Ni@NC/PEI-XC-5min, Ni@NC/PEI-XC, Ni@NC/PEI-XC-30min, Ni@NC/PEI-XC-60min, respectively.

Physical characterization

The crystalline structure of the catalysts was studied on a Rigaku D/MAX/2500PC X-ray diffractometer with a Cu K_{α} radiation source (=0.154 nm) with a scan rate of 5^{o} min^{-1} from 15^{o} to 80^{o}. The morphology and micro-structure of the catalysts were characterized on a JEM-2100PLUS transmission electron microscopy (TEM). The elemental composition and surface chemical states were probed by X-ray photo electron spectroscopy (XPS) on AXIS SUPRA spectrophotometer. Inductively coupled plasma optical emission spectroscopy (ICP-OES) was carried out on an Agilent 5110 spectrometer. H_2 adsorption isotherms were measured at 273K (0^{o}C) between 0 and 760 mm Hg on an ASAP2460/Autochem2920 analyzer.

Electrochemical characterization

The electrochemical properties of the catalysts were investigated by a three-electrode system using a rotating disk electrode. The potential was controlled by a potentiostat (Pine Instrument). A radiometer speed control unit and a rotating disk electrode radiometer from pine instrument company were used. A diameter of 5mm glassy carbon (GC) electrode, a graphite rod and Mercury/Mercury oxide (Hg/HgO) electrode were employed as working electrode, counter electrode and reference electrode, respectively. All the potentials in the work were calibrated to reversible hydrogen electrode (RHE). The catalyst ink was prepared by dispersing 5mg of catalyst in 2mL of ethanol for 15 min ultra-sonication. After that, 30μL of 5w.t.% Nafion solution was added and ultra-sonicated for 15 min. Then, 20μL of ink was drop-casted on the GC electrode. The

carbon supported catalyst loading on the GC is 255μg cm^{-2}_{geo}. The hydrogen oxidation reaction was tested in H_2 saturated 0.1M KOH with a scan rate of 1 mV s^{-1}. The HOR polarization curves was collected from -0.004 to $0.1V_{RHE}$. Accelerated degradation tests (ADT) were performed by cyclic voltammetric scanning from -0.004 to $0.1V_{RHE}$ with a scan rate of 100 mV s^{-1} for 6000 cycles in H_2-saturated 0.1M KOH. HOR polarization curves were recorded every 2000 cycle intervals. Cyclic voltammetry (CV) curves of the catalysts are recorded in N_2-saturated 0.1M KOH with a scan rate of 10 mV s^{-1} from 0 to 0.5 V_{RHE}. The electrochemical surface area (ECSA) was estimated via the Eq. S1, where Q is the integral area of the shadow area as shown in Figure S7, Q_s is the specific charge of monolayer OH adsorption on Ni, which is 514μC cm^{-2} based on the literature, and M_{Ni} is the mass of Ni on GC.

$$ECSA = Q/(Q_s \times m_{Ni}) \qquad \text{(Eq. S1)}$$

Membrane electrode assembly (MEA) fabrication and single cell testing

The membrane electrode assembly (MEA) of AEMFC with an active area of 4 cm^2 was fabricated employing Ni@NC/PEI-XC and Pt/C (40 wt. %, Johnsen Matthey Co.) as the anode and cathode catalysts, respectively. The metal loading in the anode was controlled at $1.1mg_{Ni}$ cm^{-2}, while Pt loading of 0.4 mg cm^{-2} was used for the cathode. The catalyst ink was prepared by mixing catalysts, n-propanol, anion ionomers (Alkymer®) for 30 min-ultrasonication in an ice bath. The anode catalyst ink was spray coating on gas diffusion layers (GDL, YSL-26) and then immersed in 1M NaOH solution for ion exchange. The cathode catalyst ink was spray coating on one side of the anion exchange membrane (W-25, Alkymer®). Then, the cathode catalyst coated membrane(C-CCM) was immersed in 1M NaOH solution for ion exchange. The solution was heated to 60°C and kept for 24h. After that, the C-CCM were rinsed with deionized water for several times. Afterwards, the C-CCM was sandwiched by one gas diffusion layer (GDL, YSL-26) and the anode catalyst coated GDL, and assembled in a fuel cell hardware. The single cell is operated at 80°C with feeding gas of 100% humidity. The flow rate for the H_2 and O_2 is 200 mL min^{-1} and 1000 mL min^{-1}, respectively. The backpressure for both sides is 200kPa. The performance of the single cell is evaluated on a fuel cell testing system. (TE301, Sunlaite Co.). For comparison, a MEA based on the commercial PtRu/C (30 wt. %Pt, 15 wt.%Ru, Johnsen Matthey Co.) in the anode with metal loading of $0.1mg_{Pt+Ru}$ cm^{-2} is also fabricated and measured.

Theoretical calculations

Density functional theory (DFT) calculations have been performed by the Vienna ab initio simulation package (VASP) [2, 3]. The generalized gradient approximation (GGA) of the revised Perdew–Burke–Ernzerhof (rPBE) functional [4] was used. We have chosen the projected augmented wave (PAW) method[5, 6] with a cutoff energy of 400 eV. The convergence energy of 10^{-4} eV and fore convergence criteria of 0.05eV/Å were used to realize ionic relaxations. The van der Waals (vdW) corrections have been introduced[7]. The layer at the bottom of metal was fixed, while all the other atoms relaxed. Three metal layers were used for all structures, while the layer was fixed at the bottom. Spin-polarization and non spin-polarization were both considered in calculations, as shown in Table S4, which showed a similar change of adsorption energies. And therefore, non spin-polarization was used for the following discussion.

A confined model of a (5×3) Ni(111) supercell with a (5×3) graphene overlayer, combined with a local pyrrolic N structure was structured, namely Ni-NGr-2', as shown in Figure S17. Then, we have performed additional DFT calculations, listed in Table S4. The calculated adsorption energies of intermediates on Ni-NGr-2' were all weaker than those on Ni (111), which exhibited a consistent trend with Ni-NGr-2. Some of the unsaturated C atoms of graphene overlayer in the Ni-NGr-2' structure would prefer to adsorb on the Ni (111) surface, which is possibly due to the high content of defects. It is not an apple-to-apple comparison with other models. Therefore, the Ni-NGr-2 was used to compare with other structures shown in main text, while the Ni-NGr-2' was listed in SI.

A few important elementary steps for HOR were studied considering the alkaline environment, as shown in Equations R1-R5. All the adsorption energies ($G_{ad}H^*$, $G_{ad}OH^*$ and $G_{ad}H_2O^*$) were referred to the gas phase energies of H_2O and H_2. The free energy corrections were applied on all the calculated energies at the temperature of 298 K. The solvation effect was also calculated using implicit models through VASPsol[8] calculations on Ni and Ni-NGr. The solvation effect of adsorption energies of Ni-NGr were applied on all the other confined structures. In addition, the chemical potential of OH^- was calculated by $G\ OH^- = G\ H_2O - ½\ G\ H_2$ under U=0 V vs RHE.

$$1/2\ H_2 + * \rightarrow H^* \qquad (R1)$$

$$OH^- + * \rightarrow OH^* + e^- \qquad (R2)$$

$$H^* + OH^* \rightarrow H_2O^* + * \qquad (R3)$$

$$H_2O^* \rightarrow H_2O + * \qquad (R4)$$

$$H^* + OH^- \rightarrow H_2O + * + e^- \qquad (R5)$$

Table S1. Contents of Ni in the catalysts determined from the ICP-OES measurements.

Catalyst	Content of Ni (w.t.%)
Ni/XC	35%
Ni/PEI-XC	35%
Ni@NC/PEI-XC	34%

Table S2. Comparison of the Ni@NC/PEI-XC catalyst with some state-of-the-art Ni-based electrocatalysts for HOR in alkaline media.

Electrocatalyst	Electrolyte	ECSA [$m^2\ g_{Ni}^{-1}$]	$j_{0,\ ECSA}$ [$\mu A\ cm_{Ni}^{-2}$]	$j_{0,\ m}$ [$A\ g_M^{-1}$]	$j_{k,\ m}^{50\ mV}$ [$A\ g_{Ni}^{-1}$]	Reference
Ni@NC/PEI-XC	0.1M KOH	20.41	38	7.84	24.4	This work
70% Ni/N-CNT	0.1 M KOH	10.4	28	3.5	9.3	[9]
32.5%Ni_3@h$(BN)_1$/C-700NH_3	0.1M NaOH	15.20[a]	23	3.5	-	[10]
55% Ni/SC	0.1 M KOH	16.9 ± 0.9	40.2 ± 2.8	7.44 ± 0.88	11	[11]
52.3% Ni/XC-72	0.1 M KOH	-	16 ± 2	-	5.89 ± 0.71	[12]
46.1% CeO_2(r)-Ni/XC-72	0.1 M KOH	-	38 ± 2.2	-	12.8 ± 0.27	[12]
Ni-H_2-2%	0.1 M KOH	20.39	28	24.41	50.4	[1]
Ni_3N/C	0.1 M KOH	21.3	14	12	24.38	[13]
NiO/Ni	0.1 M KOH	-	26	-	5	[14]
Ni@C-500℃	0.1 M KOH	14	32	-	-	[15]

[a] Determined by the H_2 chemisorption method.

-Data unavailable

Table S3. Comparison of the particle size, the thickness carbon shell, ECSA, specific activity and mass activity of HOR on Ni catalysts.

Electrocatalyst	Particle size [nm]	the thickness of carbon shell [nm]	ECSA [$m^2\ g_{Ni}^{-1}$]	$j_{0,\ ECSA}$ [$\mu A\ cm_{Ni}^{-2}$]	$j_{0,\ m}$ [$A\ g_M^{-1}$]	$j_{k,\ m}^{50\ mV}$ [$A\ g_{Ni}^{-1}$]
Ni/XC	7.2	-	9.37	36.9	3.46	18.3
Ni/PEI-XC	4.9	-	14.72	38.2	5.62	17.6
Ni@NC/PEI-XC-5min	4.1	-	13.90	37.1	5.17	17.5
Ni@NC/PEI-XC	3.7	0.36	20.41	38.0	7.84	24.4
Ni@NC/PEI-XC-30min	4.8	1.00	23.90	28.6	6.64	20.0
Ni@NC/PEI-XC-60min	5.0	1.43	19.30	18.1	3.39	10.3

-Data unavailable

Table S4. The calculated adsorption energies of all intermediates on different surfaces.

E_{ad}/eV	non spin-polarized			spin-polarized		
	H*	OH*	H_2O*	H*	OH*	H_2O*
Ni	-0.61	-0.33	-0.51	-0.48	-0.23	-0.48
Ni-Gr	-0.56	0.47	1.50	-0.43	0.66	1.49
Ni-NGr	-0.57	0.77	1.54	-0.45	0.88	1.50
Ni-NGr-1	-0.56	0.56	0.98	-0.43	0.65	1.01
Ni-NGr-2	-0.37	1.04	0.87	-0.27	1.23	0.91
Ni-NGr-2’	-0.38	1.16	1.51	-0.26	1.28	1.52

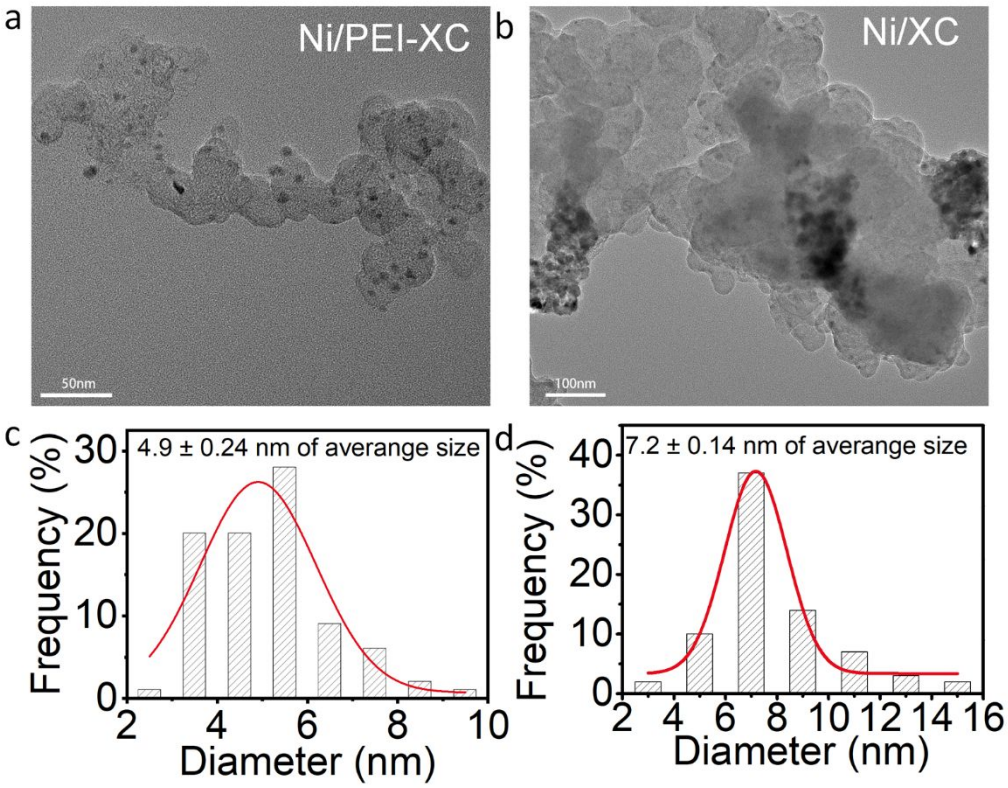

Figure S1. TEM images and the corresponding particle size distribution of Ni/PEI-XC (a) (c) and Ni/ -XC(b) (d).

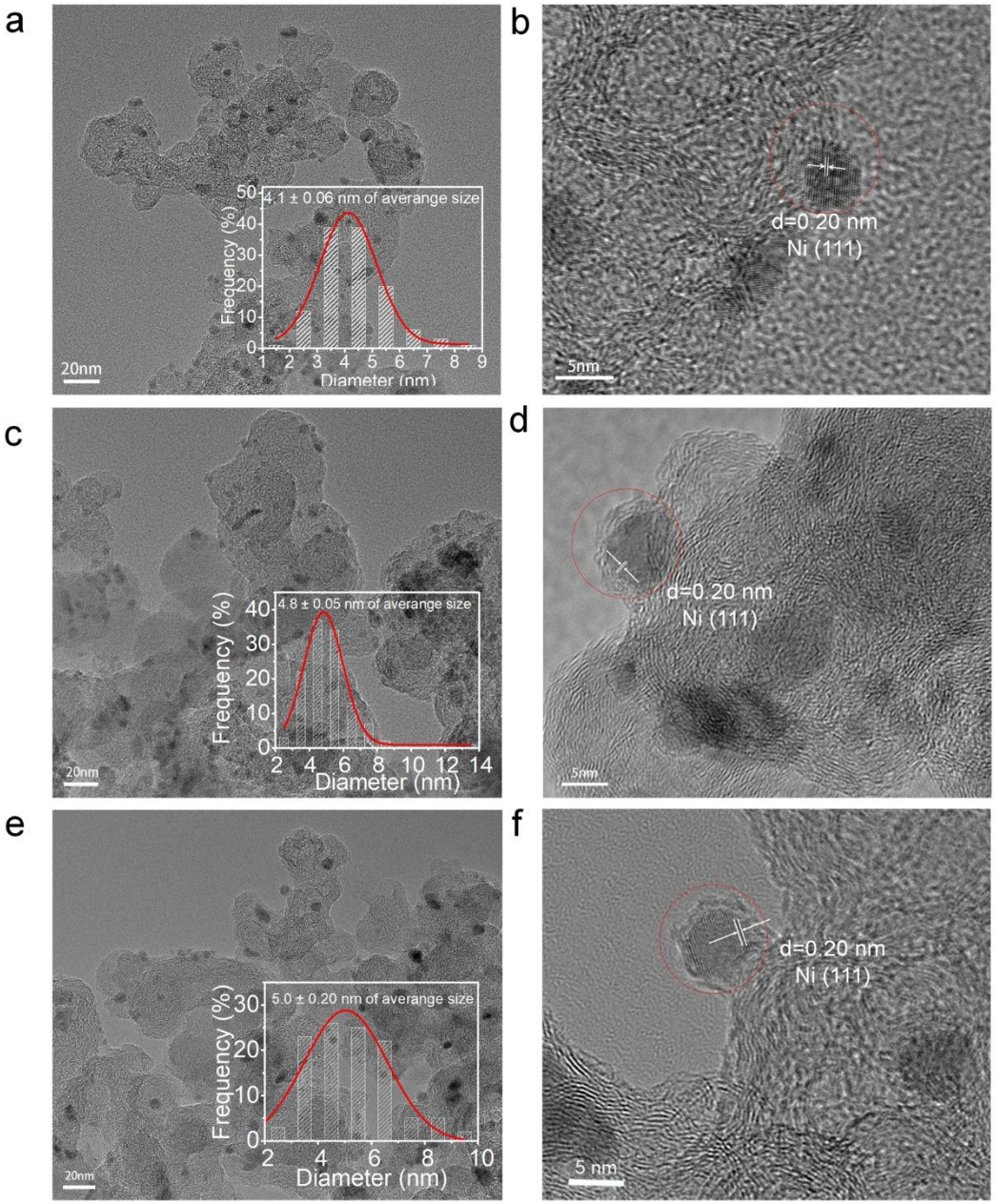

Figure S2. TEM and HRTEM images of Ni@NC/PEI-XC-5min (a, b), Ni@NC/PEI-XC-30min (c, d) and Ni@NC/PEI-XC-60min (e, f). Inserts of (a), (c) and (e) are the corresponding particle size distribution.

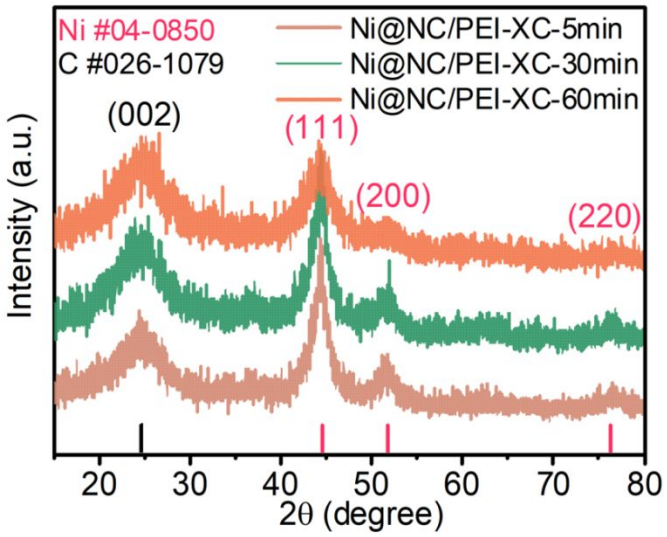

Figure S3. XRD patterns of Ni@NC/PEI-XC-5min, Ni@NC/PEI-XC-30min and Ni@NC/PEI-XC-60min.

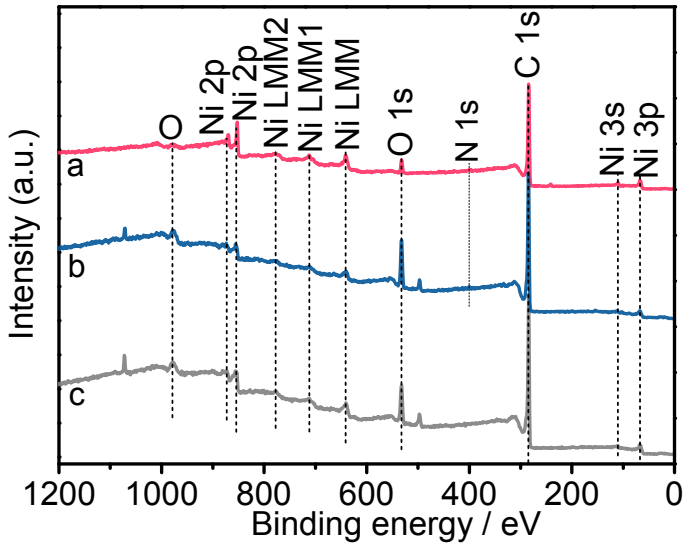

Figure S4. The survey XPS spectra of Ni@NC/PEI-XC(a), Ni/PEI-XC (b) and Ni/XC (c).

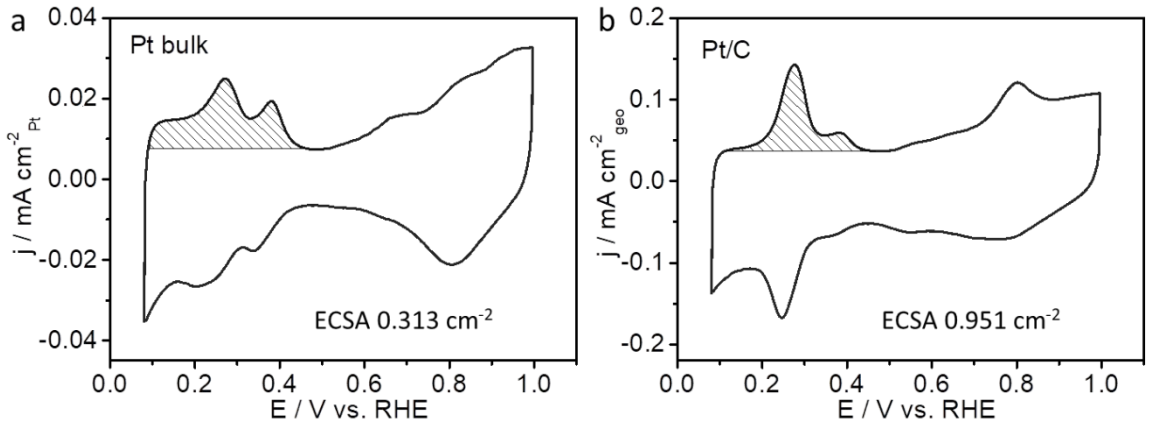

Figure S5. CV curves of Pt bulk electrode and Pt/C catalyst in N_2 saturated 0.1M KOH with a scan rate of 10 mV s^{-1}. (The loading for Pt/C on the electrode is 12.5 μg cm^{-2}_{Pt})

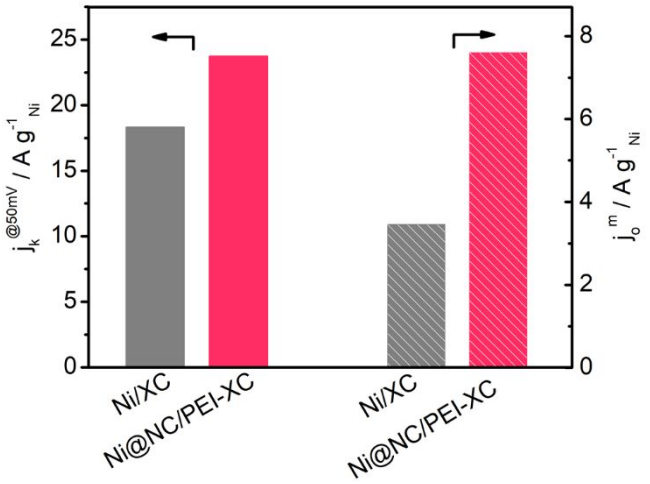

Figure S6. Kinetic current densities and exchange current densities normalized to the mass of Ni.

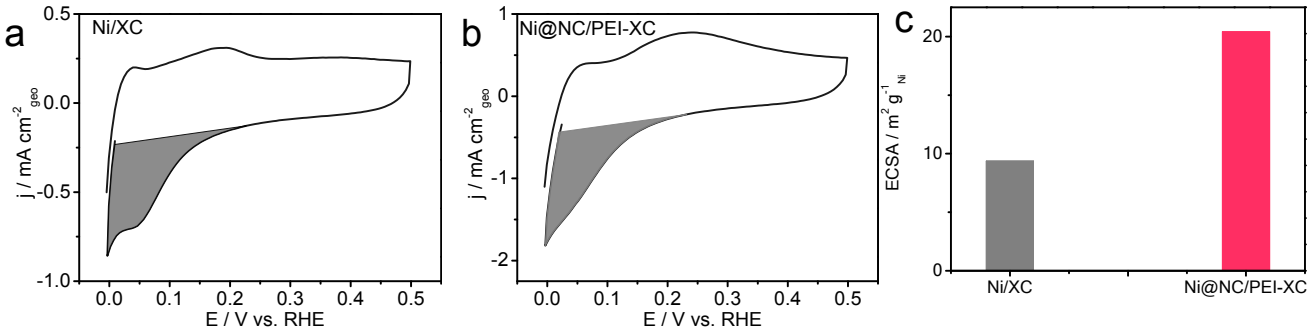

Figure S7. CV curves of (a) Ni/XC and (b) Ni@NC/PEI-XC in N_2-saturated 0.1M KOH. The scan rate is 10mV s^{-1}. (c) Comparison of the ECSA of Ni/XC and Ni@NC/PEI-XC catalysts.

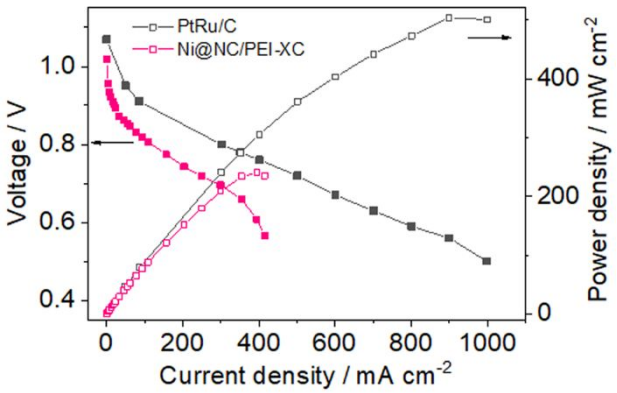

Figure S8. The discharging curves and power density curves of H_2-O_2-AEMFC with PtRu/C and Ni@NC/PEI-XC as anode catalysts at an operating temperature of 80°C. Fully humidified H_2 and O_2 with were fed at a flow rate of 200 mL min^{-1} and 1000 mL min^{-1}. PtRu/C loading is 0.1 mg $_{Pt+Ru}$ cm^{-2}, Ni@NC/PEI-XC is 1.1 mg_{Ni} cm^{-2}. The cathode catalyst loading is 0.4 mg_{Pt} cm^{-2}.

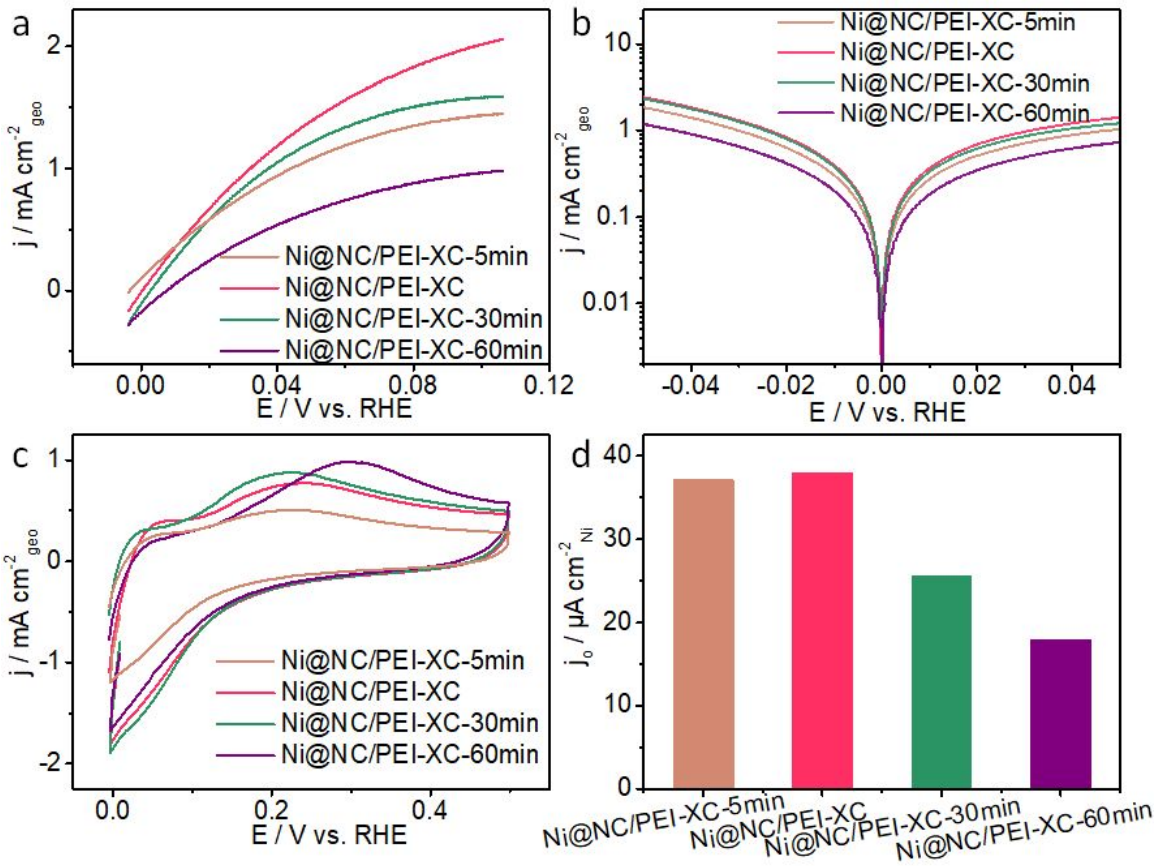

Figure S9. HOR polarization curves (a) and the Tafel plots (b), CV curves (c) of Ni@NC/PEI-XC-5min, Ni@NC/PEI-XC, Ni@NC/PEI-XC-30min and Ni@NC/PEI-XC-60min in N_2-saturated 0.1M KOH. The scan rate is 10 mV s^{-1}. Comparison of the ECSA normalized exchange current density of Ni@NC/PEI-XC-5 min, Ni@NC/PEI-XC, Ni@NC/PEI-XC-30min and Ni@NC/PEI-XC-60min catalysts. (d)

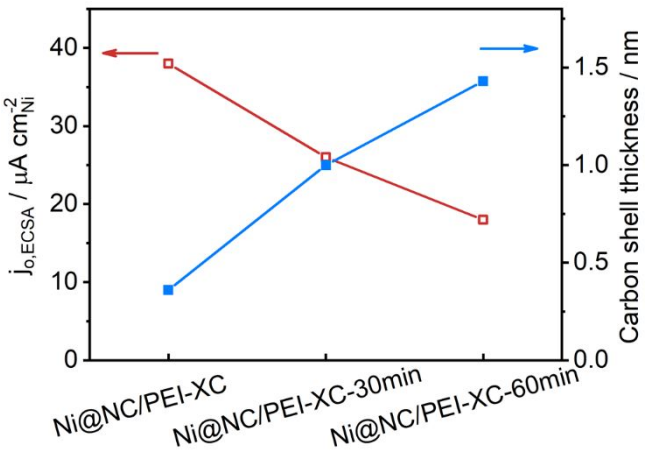

Figure S10. Dependence of specific exchange current density to the carbon shell thickness.

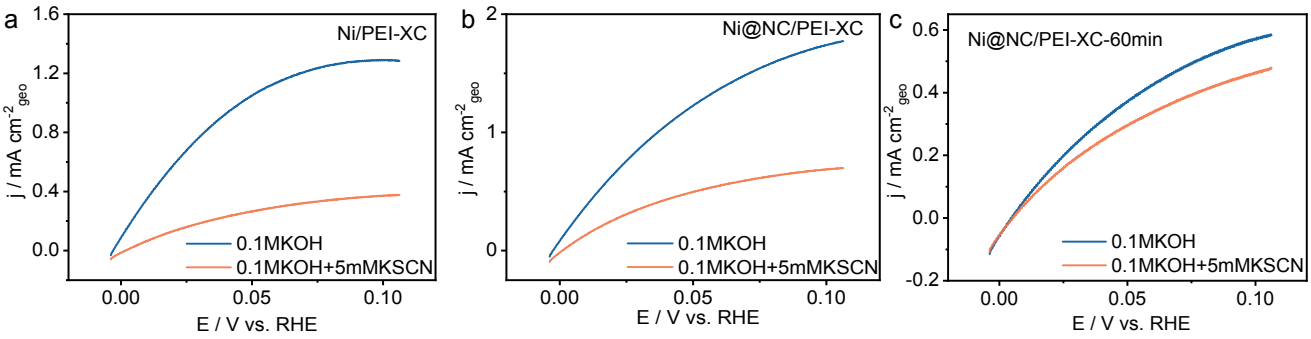

Figure S11. HOR polarization curves of Ni/PEI-XC, Ni@NC/PEI-XC and Ni@NC/PEI-XC-60min catalysts tested in H_2-saturated 0.1M KOH electrolyte containing 5mM KSCN. The scanning rate is 1 mV s^{-1}.

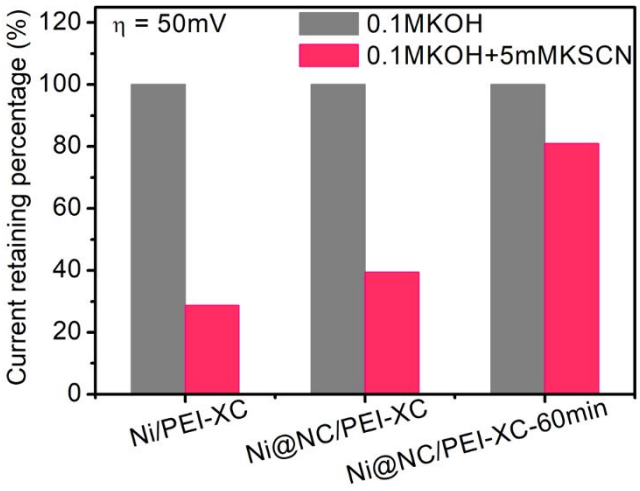

Figure S12. Current retaining percentage taken at overpotential of 50 mV in H_2-saturated 0.1M KOH electrolyte containing 5mM KSCN.

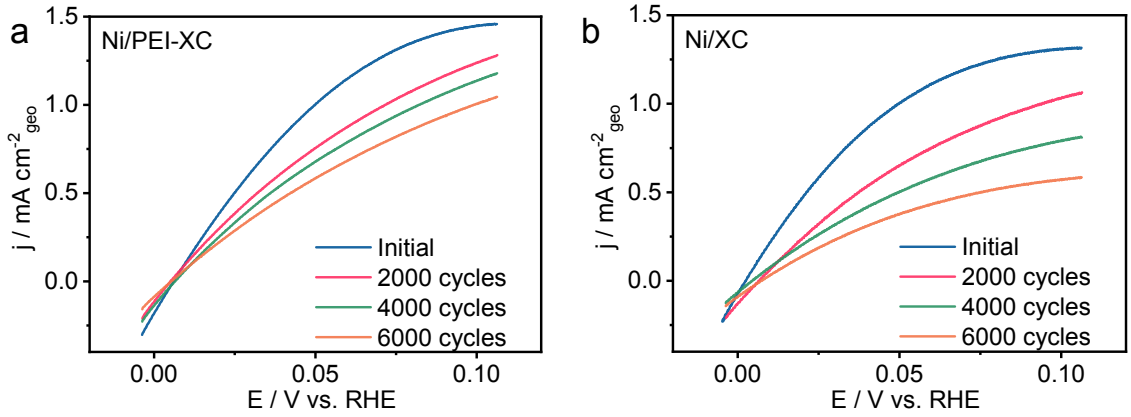

Figure S13. Polarization curves of Ni/PEI-XC (a) and Ni/XC (b) collected during the ADT test in H_2-saturated 0.1M KOH with a scan rate of 1 mV s^{-1} and a rotating rate of 2500 rpm.

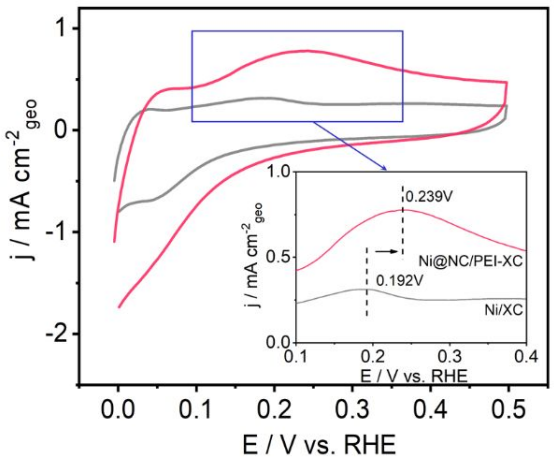

Figure S14. CV curves in N_2-saturated 0.1M KOH. The scan rate is 10mV s^{-1}.

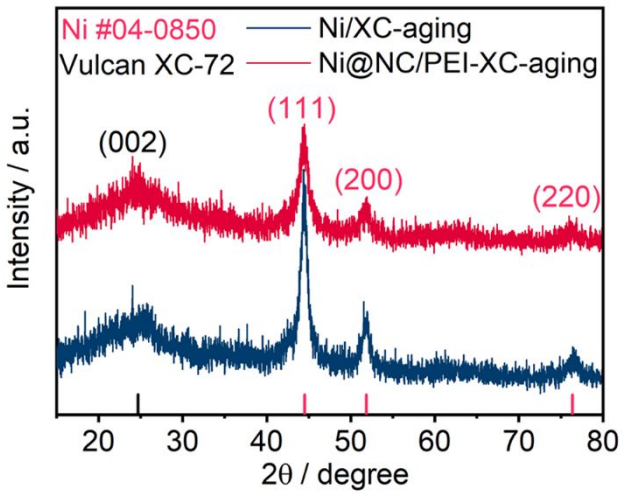

Figure S15. XRD patterns of catalysts after HOR durability test.

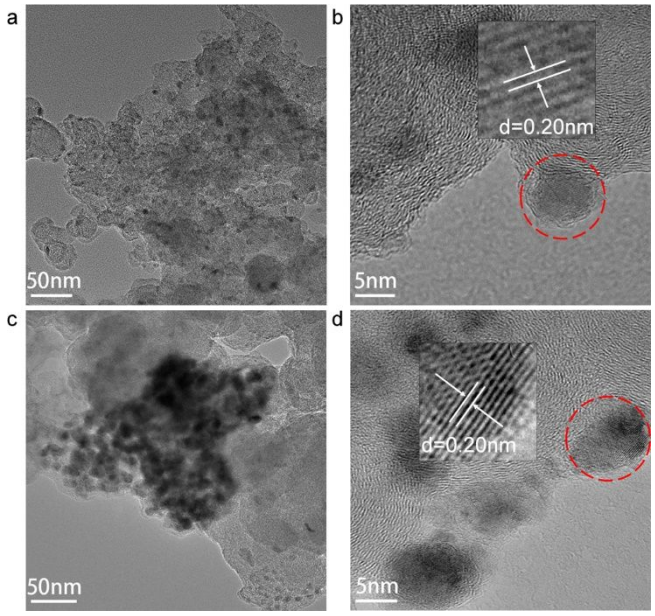

Figure S16. TEM and HRTEM images of Ni@NC/PEI-XC(a)(b) and Ni/XC(c)(d).

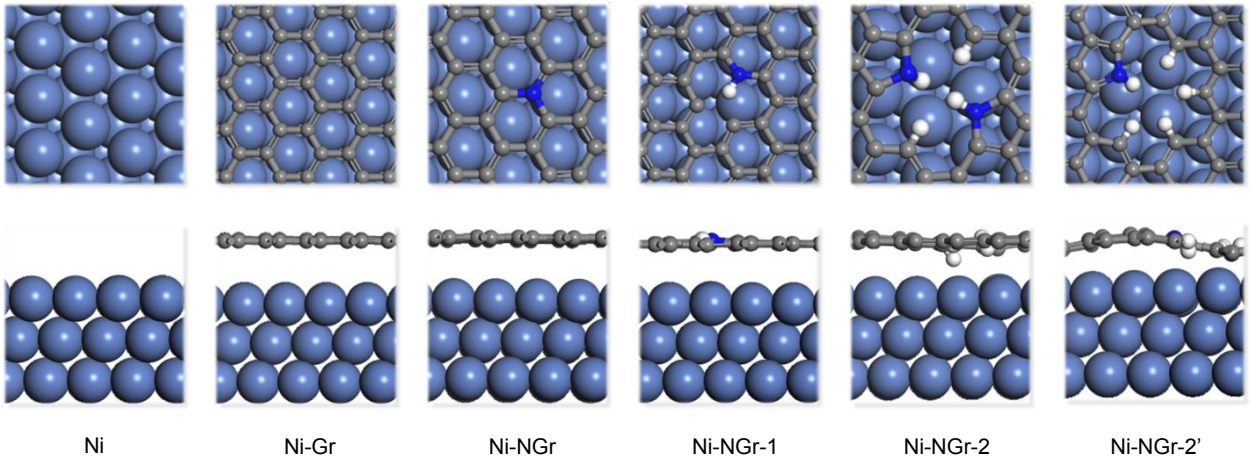

Figure S17. The top and side view of the theoretical structures.

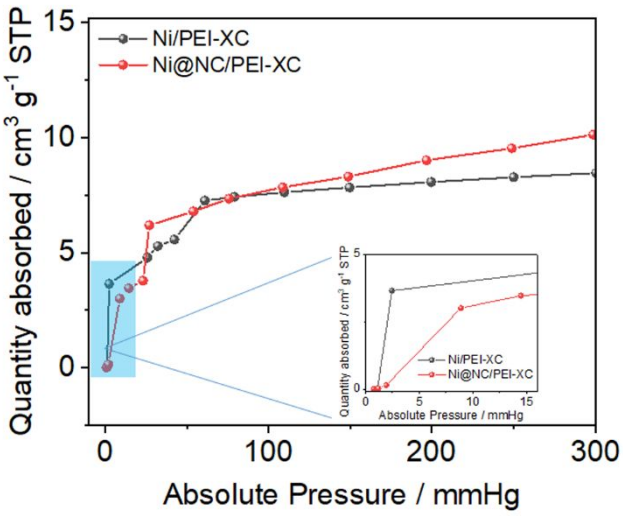

Figure S18. H_2 adsorption isotherm curves on Ni/PEI-XC and Ni@NC/PEI-XC. The insert is the enlarged view of low-pressure region.

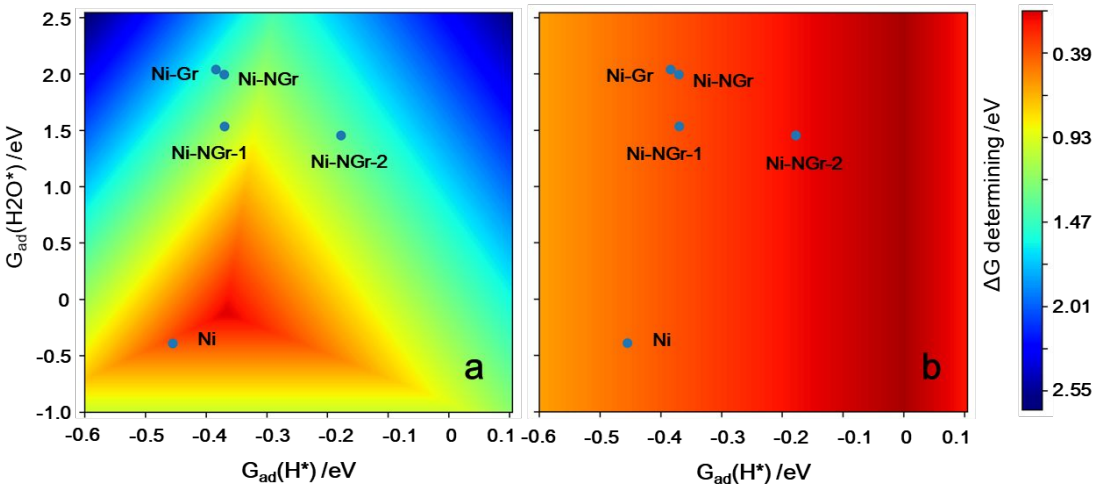

Figure S19. HOR activity map for different reaction pathways. (a) Reaction pathway is R1→R2→R3→R4. (b) Reaction pathway is R1→R5. (R1-R5 are displayed in Experimental Section in this Supporting information.)

References

(1) Ni, W. Y.; Wang, T.; Schouwink, P. A.; Chuang, Y. C.; Chen, H. M.; Hu, X. L. Efficient Hydrogen Oxidation Catalyzed by Strain-Engineered Nickel Nanoparticles. *Angew. Chem. Int. Ed.* **2020***, 59,* 10797−10801.
(2) Kresse, G.; Furthmüller, J. Efficiency of Ab-Initio Total Energy Calculations for Metals and Semiconductors Using a Plane-wave Basis Set. *Comput. Mater. Sci.* **1996,** *6*, 15-50.
(3) Kresse, G.; Hafner, J. Ab Initio Molecular-Dynamics Simulation of the Liquid-Metal-Amorphous-Semiconductor Transition in Germanium. *Phys. Rev. B* **1994,** *49*, 14251-14269.
(4) Perdew, J. P.; Burke, K.; Ernzerhof, M. Generalized Gradient Approximation Made Simple. *Phys. Rev. Lett.* **1996,** *77*, 3865-3868.
(5) Blöchl, P. E.; Jepsen, O.; Andersen, O. K. Improved Tetrahedron Method for Brillouin-Zone Integrations. *Phys. Rev. B.* **1994,** *49*, 16223-16233.
(6) Kresse, G.; Joubert, D. From Ultrasoft Pseudopotentials to the Projector Augmented-Wave Method. *Phys. Rev. B.* **1999,** *59*, 1758-1775.
(7) Grimme, S.; Antony, J.; Ehrlich, S.; Krieg, H. A Consistent and Accurate Ab Initio Parametrization of Density Functional Dispersion Correction (DFT-D) for the 94 Elements H-Pu. *J. Chem. Phys.* **2010,** *132*, 154104.
(8) Mathew, K.; Sundararaman, R.; Letchworth-Weaver, K.; Arias, T. A.; Hennig, R. G. Implicit Solvation Model for Density-Functional Study of Nanocrystal Surfaces and Reaction Pathways. *J. Chem. Phys.* **2014,** *140*, 084106.
(9) Zhuang, Z.; Giles, S. A.; Zheng, J.; Jenness, G. R.; Caratzoulas, S.; Vlachos, D. G.; Yan, Y. Nickel Supported on Nitrogen-Doped Carbon Nanotubes as Hydrogen Oxidation Reaction Catalyst in Alkaline Electrolyte. *Nat. Commun.* **2016,** *7*, 10141.
(10) Gao, L.; Wang, Y.; Li, H.; Li, Q.; Ta, N.; Zhuang, L.; Fu, Q.; Bao, X. A Nickel Nanocatalyst Within a h-BN Shell for Enhanced Hydrogen Oxidation Reactions. *Chem. Sci.* **2017,** *8*, 5728-5734.
(11) Yang, F. L.; Bao, X.; Zhao, Y. M.; Wang, X. W.; Cheng, G. Z.; Luo, W. Enhanced HOR Catalytic Activity of PGM-Free Catalysts in Alkaline Media: the Electronic Effect Induced by Different Heteroatom Doped Carbon Supports. *J. Mater.Chem. A.* **2019,** *7*, 10936-10941.
(12) Yang, F.; Bao, X.; Li, P.; Wang, X.; Cheng, G.; Chen, S.; Luo, W. Boosting Hydrogen Oxidation Activity of Ni in Alkaline Media through Oxygen-Vacancy-Rich CeO_2/Ni Heterostructures. *Angew. Chem. Int. Ed.* **2019,** *58*, 14179-14183.
(13) Ni, W. Y.; Krammer, A.; Hsu, C. S.; Chen, H. M.; Schuler, A.; Hu, X. L. Ni_3N as an Active Hydrogen Oxidation Reaction Catalyst in Alkaline Medium. *Angew. Chem. Int. Ed.* **2019,** *58*, 7445-7449.
(14) Yang, Y.; Sun, X. D.; Han, G. Q.; Liu, X.; Zhang, X. Y.; Sun, Y. F.; Zhang, M.; Cao, Z.; Sun, Y. J. Enhanced Electrocatalytic Hydrogen Oxidation on Ni/NiO/C Derived from a Nickel-Based Metal-Organic Framework. *Angew. Chem. Int. Ed.* **2019,** *58*, 10644-10649.
(15) Gao, Y.; Peng, H.; Wang, Y.; Wang, G.; Xiao, L.; Lu, J.; Zhuang, L. Improving the Antioxidation Capability of the Ni Catalyst by Carbon Shell Coating for Alkaline Hydrogen Oxidation Reaction. *ACS Appl. Mater. Interfaces* **2020,** *12*, 31575-31581.